Chemically Functionalized Gold Nanosphere-Blended Nematic Liquid Crystals for Photonic Applications

Bhupendra Pratap Singh, Samiksha Sikarwar, Shikha Agarwal, Dharmendra Pratap Singh, Kamal Kumar Pandey, Rajiv Manohar

ACS OMEGA

http://pubs.acs.org/journal/acsodf

Article

Chemically Functionalized Gold Nanosphere-Blended Nematic Liquid Crystals for Photonic Applications

Bhupendra Pratap Singh,[⊥] Samiksha Sikarwar,[⊥] Shikha Agarwal, Dharmendra Pratap Singh, Kamal Kumar Pandey,* and Rajiv Manohar*

Cite This: *ACS Omega* 2023, 8, 2315−2327

Read Online

ACCESS | Metrics & More | Article Recommendations | Supporting Information

ABSTRACT: A demand for functional materials that are capable of tailoring light-emissive properties has apparently been rising nowadays substantially for their utilization in organic optoelectronic devices. Motivated by such promising characteristics, we present highly emissive as well as aggregation-induced emission (AIE) electroluminescent composite systems composed of a nematic liquid crystals (NLC) blended with polyethylene-functionalized gold nanospheres (GNSs). The major findings of this study include superior electro-optical properties such as threshold voltage reduction by around 24%. The fall time is reduced by 11.50, 30.33, 49.33, and 63.17% respectively, and rotational viscosity is reduced by 13.86, 32.77, 36.97, and 49.58% for 5.0×10^{11}, 5.0×10^{12}, 2.5×10^{13}, and 5.0×10^{13} number of GNS-blended liquid crystal (LC) cells. The increased UV absorbance and greatly enhanced luminescence properties have been attributed to surface plasmon resonance near the surface of GNSs and AIE effect risen due to agglomeration of the capping agent with the NLC molecules respectively, and these characteristics make them suitable for new-age display applications.

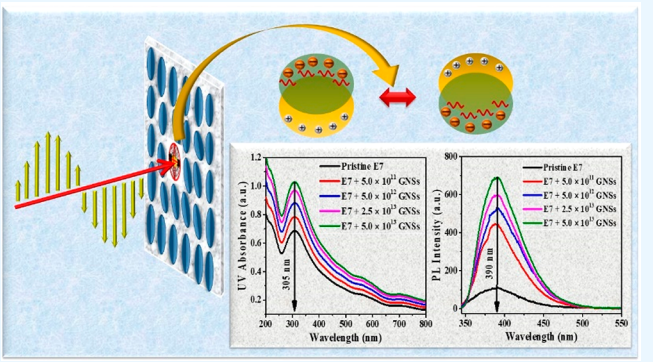

1. INTRODUCTION

Nanomaterial research has led a significant impact on the emerging field of materials science over the last few decades. The enormous influence of nanomaterials on modern technology is solely due to their size-dependent electronic, optical, magnetic, and chemical properties. Because of their potential scientific and technological relevance, investigation into micro/nano-scale colloids dispersed in liquid crystals (LCs) has stimulated enormous interest within this framework.[1−3] The best examples of anisotropic fluids are LCs, which have proven to be an appropriate medium for studying the interaction between colloidal particles and LCs. A few theoretical and experimental studies on colloidal particles dispersed in LCs have been conducted, with the shape/size of colloids and the self-assembling nature of the LCs being heavily considered.[1,4−7]

Topological defects (Saturn rings, hedgehog space, and boojums) are produced by the dispersed colloidal particles' elastic deformation of the LC, which further mediates the long-range anisotropic interactions among colloids, resulting in their controlled organization within the LC matrix. Moreover, the emergence of topological defects offers a framework for better understanding the dynamics of LC molecular alignment in the presence of colloidal particles. Furthermore, the billions of dollars' worth LC technology has recently partnered with nanotech to alter the physical properties of LCs via nanocrystals and vice versa. Use of metal nanoparticles (MNPs) to customize the characteristics of LCs and LCs to tune the properties of MNPs, for example, has finally opened numerous avenues for these LC−MNP composites to be used in a variety of opto-electronic devices. Gold nanoparticles (GNPs) dispersed in LCs have been extensively studied and found to be critical for technological applications. The optical performance of display technologies, such as brightness and efficiency, is influenced by luminescence, which is a key parameter of GNPs. As a result, techniques to enhance the luminescence intensity from the perspective of GNP materials and external constructions have been implemented.[8−10] Several approaches, including surface passivation of GNP materials, localized surface plasmon resonance, scattering-based enhancement, and increased light extraction, are discussed in the following sections. Furthermore, dynamic modulation is briefly discussed.[11,12]

The surface features (such as surface imperfections) and dispersion stability of colloidal GNPs have a strong influence

Received: October 18, 2022
Accepted: December 19, 2022
Published: January 3, 2023

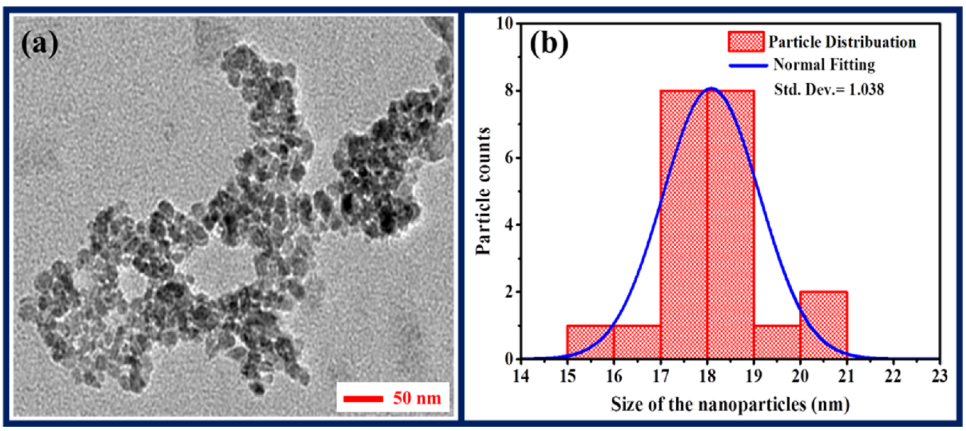

Figure 1. (a) TEM image and (b) histogram for diameter distribution of the PEG-functionalized GNSs.

on their fluorescence emission. The luminescence increase is aided by establishing effective surface passivation technologies and screening suitable surface ligands.[13−15] For example, Chang et al.[3] reported 64% increase in photoluminescence (PL) intensity in liquid crystals 5CB after doping appropriate amounts of GNPs. Biradar and co-workers[16] reported a detailed study on GNP-dispersed deformed helix ferroelectric liquid crystals (DHFLCs) which clearly showed sevenfold and ninefold enhancement in the PL intensity with 20 and 100 μL of GNP solution. Chaudhry et al.[17] also reported a comprehensive study on thermal, electro-optical, and PL studies of GNP-dispersed nematic LCs (EBBA) and observed a significant enhancement of PL intensity. This established the resonance condition by increasing the energy transfer effect between the pristine and dispersed nematic liquid crystals (NLCs). Mohajerani and co-workers[18] fabricated an electrically programmable narrow band PL emitted by a hybrid plasmonic-Fabry Perot cavity. A single metal thin film and a plasmonic gold nanoisland (NI) layer are used as a reflector of this cavity. Unlike a thick metal layer, the NI layer significantly improves the quality of the cavity modes in a specific plasmonic spectrum area. In an LC system composed of GNPs and CdSe quantum dots (QDs), Chen et al.[19] demonstrated to adjust the coupling between localized surface plasmon of GNPs and excitons of CdSe QDs by embedding both nanomaterials in an LC cell. Abdullah et al. studied linear and nonlinear optical properties of LCs.[20] Self-defocusing and saturable absorption were observed in the MBBA LC doped with GNPs. Cyanobiphenyl LCs doped with GNPs dramatically affect the display parameters and mesophase stability of NLCs and also provide a lower switching voltage and time.[21] Chaudhary et al. reported behavior of surface plasmon resonance (SPR) in calamitic LCs doped with GNPs.[22] However, it was examined by different scientific groups that various shapes, sizes, and natures of NPs dispersed in LCs exhibit different capabilities to capture the ions, enhance the alignment of LCs, and therefore, tune their characteristics.[23−29] The NLC doped with 2 nm GNPs significantly decreases the threshold voltage (up to 60%) and up to 80% decrease in the rise time in photonic crystal fiber.[30] Nevertheless, a challenging but crucial requirement is dispersing NPs in the LC matrix. Dispersion of NPs in the LC matrix is still a challenging task because it is hard to find a suitable organic solvent for particular NPs, strong van der Waals interactions between adjacent NPs promoting clustering, and their nonuniform dispersion. Likewise, complete evaporation of the solvent from the LC−NP dispersed system and stabilization against coagulation of these colloids are usually attributed to the presence of negative charges onto the surface of "naked" particles, and their role in the NP stability is a matter of debate. GNPs should be functionalized to be highly dispersible in the host LC. The assembling of these NPs in clusters can be modulated by making use of copolymer ligands on their surface which is an important phenomenon, considering the fact that the change in arrangement of NPs in any cluster would change the optical and electro-optical properties of the system.[31] In the past few years, GNPs have become commercially available in various sizes (5−250 nm) with a variety of stabilizers.[32] Various early studies have been reported in which various preparation procedures have been employed to manufacture GNPs in a variety of forms, sizes, and stabilizing media. However, the dielectric and electro-optical properties of the LC−GNP composite system as a function of polyethylene glycol (PEG)-functionalized gold nanosphere (GNS) concentration are yet to be thoroughly investigated.

In the present work, we attempt to investigate UV-shielding characteristics and enhancement in PL intensity of pristine and GNP-dispersed NLCs. The dielectric and electro-optical characteristics of a pristine and PEG-functionalized GNS-dispersed systems have also been systematically discussed.

2. MATERIALS AND METHODS

2.1. Nematic Liquid Crystals. The nematic LC E7 (Merck KGaA, Darmstadt, Germany, T_{NI} = 60.5 °C) was used in the experiment (CAS No. 40817-08-1). The nematic LC E7 mainly consists of LC monomers 5CB (51%), 7CB (25%), 8OCB (16%), and 7CT (8%). The molecular structure of each monomer is presented in the Supporting Information (see Figure S1a). The E7 LC mixture had a positive dielectric anisotropy ($\Delta\varepsilon$) of 14.1, a birefringence (Δn) of 0.22, a nematic−isotropic phase transition temperature (T_{NI}) of 60.5 °C, a rotational viscosity (γ) of 232.6 mPa·s, and elastic constant K_{11}, K_{22}, and K_{33} values of 11.1, 5.9, and 17.1 pN, respectively, at 20 °C.

2.2. Synthesis of PEG-Functionalized GNSs. *2.2.1. Chemicals.* All glassware was cleansed with aqua regia (HNO_3:HCl in ratio 1:3), rinsed with distilled water, and dried overnight at 80−100 °C prior to synthesis. Magnetic flees were sonicated in ethanol for 15 min before being rinsed in deionized (DI) water and dried. Sigma-Aldrich USA provided the chloroauric acid ($HAuCl_4{\cdot}3H_2O$), low-molecular mass PEG (5 kDa), and sodium citrate. Deionized and ultrafiltered

https://doi.org/10.1021/acsomega.2c06718
ACS Omega 2023, 8, 2315−2327

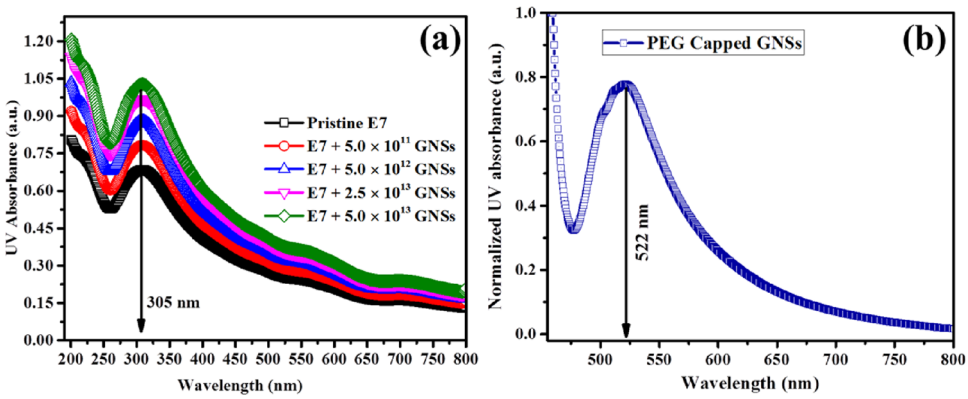

Figure 2. (a) UV−visible absorbance spectra of pristine E7 and GNS-blended LC cells at various GNS concentrations and (b) UV−visible absorbance spectrum for pristine GNSs.

water (18.1 MΩ cm) (DIUF water) was procured from Sigma-Aldrich USA and used as received.

2.2.2. Synthesis. One hundred milliliters of 0.01 wt % $HAuCl_4$ was heated to a boil in a 250 mL round-bottomed flask equipped with a condenser with vigorous stirring. Then, 2 mL of 1 wt % sodium citrate was immediately added, causing the color to change from blue to burgundy. The resultant solution was cooled to room temperature (RT) after 10 min of stirring at the same temperature yielding citrate-capped GNSs. To synthesize GNSs with PEG coating, low-molecular mass PEG was added to previously synthesized citrate-capped GNS solutions at RT. After adding the required quantity of PEG, the solution was stirred at RT for 2 h to allow the citrate molecules to completely exchange with PEG. The PEG-coated GNSs that resulted were collected by centrifugation at 16,800*g* for 30 min and washed twice with distilled water to remove any unattached PEG or other reactants.[33,34] The physical appearance of the resulting GNS suspension is crimson red in color. The schematic illustration of PEG-capped GNS is presented in the Supporting Information (see Figure S1b).

2.2.3. Characterization. Figure 1a shows the transmission electron microscopy (TEM) images, and Figure 1b depicts the histogram for diameter distribution of highly purified PEG-functionalized GNSs. The results revealed that the resulting GNPs have highly purified PEG-functionalized GNSs showing an average diameter of 18 ± 1.5 nm with a standard deviation ∼1.038 and a coefficient of variation $\left(\frac{\text{Deviation}}{\text{Mean}} \times 100\right)$ is <12%. The SPR of the PEG-coated GNSs is ∼521.5 ± 2 nm, particle concentration (per mL) for optical density (OD) (using a 1 cm path length cuvette) = 1 is ∼5.0 − 8.6 × 10^{11} nanospheres, mass concentration (mg/mL) for OD = 1 is 0.050−0.056, particle molar concentration for OD = 1 is ∼0.8 − 1.5 × − 9, zeta potential −4 ± 5 mV, and pH 6−8.

2.3. Sample Holder Preparation. A 5 μm-thick empty cell composed of two indium-tin-oxide (ITO) glass substrates was constructed. Our previously published work contains a detailed description of the sample cell fabrication process.[29,35,36] The thickness was confirmed by the optical interferometric method and found to be ∼5.2 ± 0.05 μm. The concentration was set to 0, 5.0 × 10^{11}, 5.0 × 10^{12}, 2.5 × 10^{13}, and 5.0 × 10^{13} nanospheres in pure LC. The LC mixtures were heated above the isotropic temperature to fill in the empty cell uniformly via capillary action and successively cooled down to the nematic phase.

2.4. Experimental Details and Measurement Techniques. Various instruments and experimental techniques used in the present investigation are discussed below: a polarizing optical microscope (DM EP, LEICA, Germany) integrated with a temperature controller (T95-PE, Linkam, UK) was used to record optical texture and observe T_{NI} of pure E7 and LC−GNS composite system. The transmission spectra with the variation of wavelength were recorded using computer-operated commercial software ISM-Lux by Isuzu Optics corp. Taiwan integrated with a white light source. The response time was calculated by the optical switching technique of pure E7 and LC−GNS composite system at RT. The experimental setup and measurement techniques for transmission versus voltage ($T-V$) curve and response time were reported in our previously published articles.[29,35] The pre-tilt angles of homogeneously aligned (HA or electrically controlled birefringence (ECB)) cells and vertically aligned (VA) LC cells of pure E7 and LC−GNS composite systems were calculated using the crystal rotation method.[37] For all concentrations, the pure E7 and E7/GNS-blended LC cells were estimated to be 2.0° and 88.7° for HA and VA cells, respectively. The dielectric spectra of the HA and VA of pure E7 and LC−GNS composite systems were measured using an LCR meter (Hioki 3532-50, Japan) with an applied alternating current (AC) field of 0.01 V/μm, and the frequency was varied from 42 Hz to 5.5 MHz for high-frequency dielectric analysis to obtain the real and imaginary parts of dielectric permittivities and dielectric anisotropy. The Δn of the LCs was derived with the phase retardation technique.[29,36] Additionally, for the purpose of absorption measurements using the dichroism method, optical-grade potassium chloride (KCl) drilled windows (discs) were used as a substrate (by Alkor Technologies, St Petersburg, Russia) instead of indium-tin-oxide (ITO)-coated glass plates because the transparency of the ITO layer is poor. For the absorption measurement, only a thin alignment layer (∼1600 Å; homogeneous polyamide (HA-PI) AL-1426CA (Daily Polymer Corp., Taiwan)) was deposited onto the substrate without an ITO conductive electrode.

3. RESULTS AND DISCUSSION

3.1. Optical Spectroscopy. Absorption spectroscopy is an effective and nondestructive technique for the exploration of optical properties of the metallic nanoparticle-blended nematic LC matrix. In order to explore the mechanism behind the interaction of PEG-capped GNSs with the E7 liquid crystal

https://doi.org/10.1021/acsomega.2c06718
ACS Omega 2023, 8, 2315−2327

under the influence of electromagnetic (EM) waves, we have conducted UV−visible absorption spectroscopy of E7 in the pristine form as well as dispersed with varying concentrations of PEG-functionalized GNSs, and the spectra are illustrated in Figure 2a where it is evident that the primary absorption band centered at 305 nm basically remains unchanged with increasing concentrations of GNSs in the nematic system; however, the system undergoes a hyperchromic shift (i.e., enhancement of absorption of the incident EM wave through the system) with the increment of the number of GNSs in it.

This increased absorbance can be attributed to the plasmonic nature of GNSs, distinguished by the unique phenomenon of SPR that occurs as a consequence of photon confinement within the small size of nanospheres and enhances their radiative and nonradiative properties. On exposing GNSs to light, the collective coherent oscillation of the conduction band electrons takes place in the metal on account of the interaction between metal and oscillating electromagnetic field of incident light waves. The oscillation of free electrons leads to separation of charge from the ionic lattice which consequently leads to the formation of dipole oscillation along the direction of the electric field vector of light. At a specific frequency of incident wave, the amplitude of these oscillations reaches maxima and is known as SPR due to which the incident wave gets strongly absorbed. For pristine GNSs, this phenomenon of SPR occurs at a resonant wavelength of 522 nm as demonstrated in Figure 2b but when these nanospheres have been inserted in the matrix of NLC E7 molecules, the position of this SPR band gets affected owing to the dielectric constant of the surrounding liquid crystalline material and the change in electron charge density on the surface of GNSs due to the interaction between the capping agent and molecules of E7, as theoretically described by Mie theory.[38] As an outcome, the incorporation of GNSs increases the optical path traversed by the incident electromagnetic wave inside the nematic matrix, and henceforth, the ability of the system to absorb those incoming radiations gets enhanced. This can schematically be represented as we have done in Figure 3. The enhanced absorption of EM waves also indicates the possibility that GNS-blended nematic composites might be a suitable approach for photothermal therapy in the biomedical sector as the system has greater tendency to efficiently convert the incident energy to heat in order to cause cell and tissue destruction.[39]

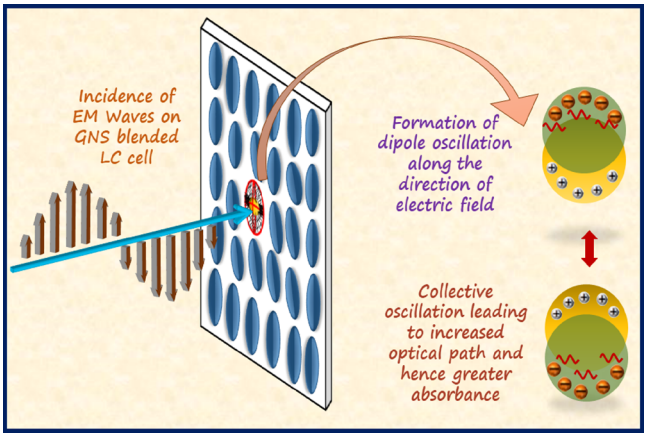

Figure 3. SPR in GNSs owing to their interaction with incident electromagnetic waves, leading to enhanced UV absorbance in the system.

Furthermore, PL spectra of pristine E7 and GNS-blended LC cells were recorded at an excitation wavelength of 305 nm to explore the impact of addition of increasing concentrations of GNSs on the luminescent characteristics of pristine E7, and the same has been illustrated in Figure 4a. In the absence of GNSs, the pure E7 exhibited weak PL emission at 390 nm. However, when the concentration of PEG-capped GNSs was increased from 0 to 5.0×10^{11} number of GNSs, the luminescence of the mixture gets substantially enhanced, as evidenced by the PL spectra in Figure 4a. At this concentration, the emission intensity with maxima at a wavelength of 390 nm was approximately 4-fold higher than that in the absence of GNSs. Further increments in the GNS concentration from 5.0×10^{11} to 5.0×10^{13} number of GNSs have increased the luminescent emissivity continually, and ultimately, we have achieved around 6.5 times enhancement of PL emissivity due to dispersion of PEG-capped GNSs in nematic LC E7. Such huge enhancement may be accredited to the aggregation-induced emission (AIE) effect in the system. This phenomenon is characterized by the aggregation of any appropriate luminogen in a system consisting of weak fluorophores or even nonluminescent molecules and leads to enhancement of their emission considerably.[40] In our case, the capping agent PEG acts as an AIE luminogen with high solid-state efficiency, and the functionalization of GNSs with this agent leads to the AIE effect in PL emission. This capping agent interacts with surrounding LC molecules in such a way that the long polymeric chains of polyethylene glycol form aggregates with E7 molecules and hence confines the metal nanosphere inside it efficiently, thereby preventing the mutual aggregation and clustering of GNSs with each other usually generated by strong van der Waals interactions between them. This can also be ensured by the polarized optical micrographs illustrated in the Supporting Information (see Figure S2).

Additionally, the electroluminescence (EL) of LC E7, without and with the dispersion of GNSs in different concentrations, has been recorded at voltages varying from 0 to 10 V, and Figure 5 shows these EL spectra. For the pure E7 LC cell, no change in the EL spectrum occurred with increasing voltage, and the emission peak was at the position same as that obtained in the PL spectrum, indicating that the system is nonelectroluminescent. In fact, with increasing concentration of GNSs in the NLC matrix, the system becomes electroluminescent owing to the interaction of oscillating electron waves in GNSs with the light traversing through the composites. At optimum concentration (i.e., 5.0×10^{13} number of GNSs), the rising voltage shifts the EL spectrum toward a longer wavelength region in the visible regime of the EM spectrum, and the emission peak at 403 nm has been observed at 10 V for this concentration. Furthermore, no deterioration in the spectra shape has been observed up to this voltage.

One of the most favorable outcomes of these concentration-dependent experiments is that there is a slight change in the "International Commission on Illumination" (CIE) coordinates of the pure E7 LC cell with the incorporation of GNSs in the system (Calculated by using PL spectra and Color-Calculator software, Version 7.77 by OSRAM Sylvania, Inc., United States). However, no change in these coordinates has been observed with varying concentrations of GNSs, exhibiting a stable output at (0.1645, 0.0326) and promoting deep blue

https://doi.org/10.1021/acsomega.2c06718
ACS Omega 2023, 8, 2315−2327

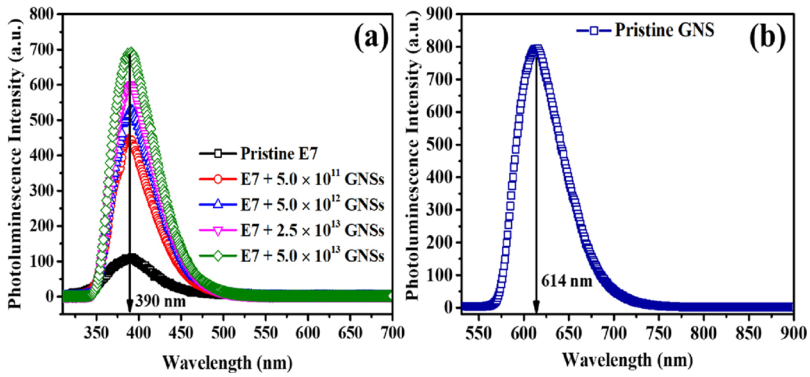

Figure 4. (a) PL spectra of pristine E7 and GNS-blended LC composite systems at various GNS concentrations, and (b) PL spectra of pristine GNSs.

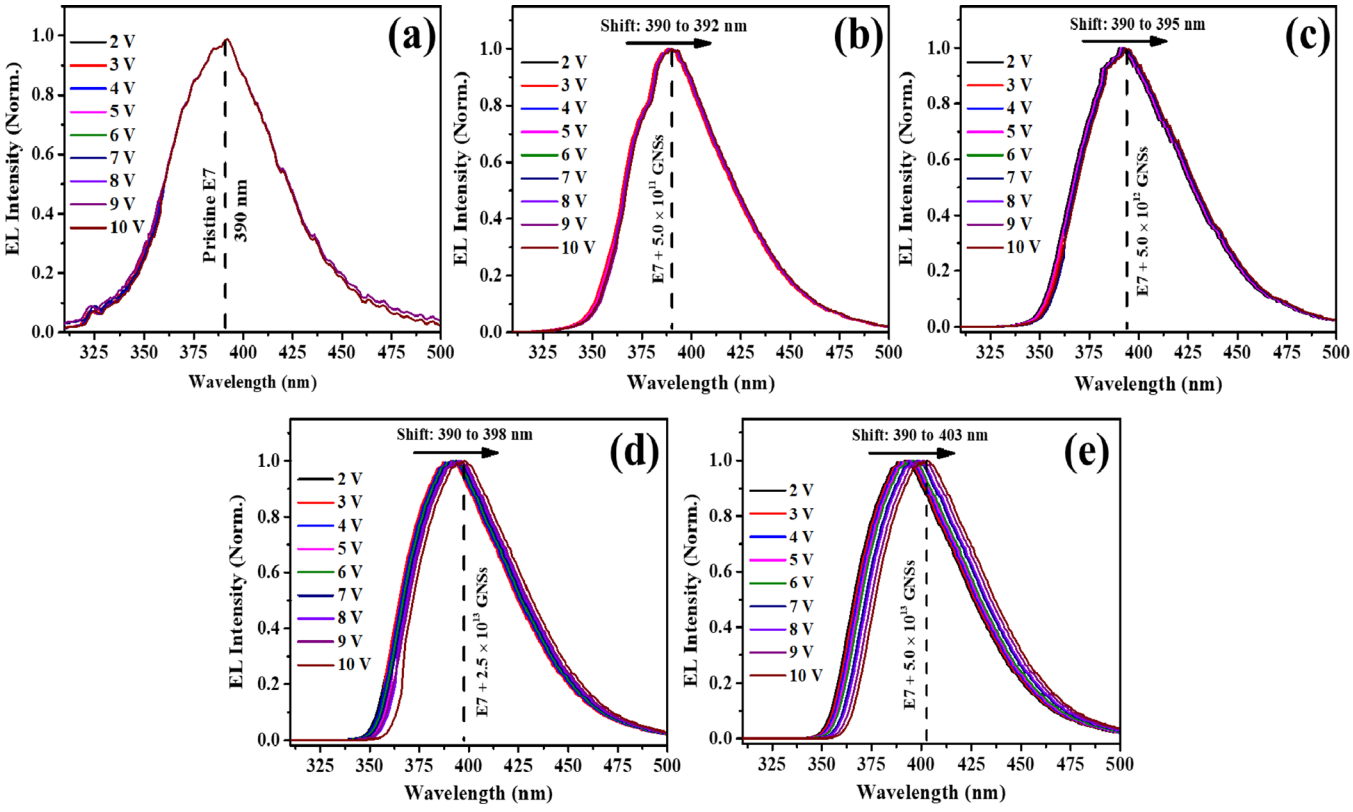

Figure 5. Electroluminescence spectra of (a) pristine E7 LC and (b) 5.0×10^{11}, (c) 5.0×10^{12}, (d) 2.5×10^{13}, and (e) 5.0×10^{13} number of the GNS-blended E7 system under voltages varying from 2 to 10 V.

emission as per the standards of European Broadcasting Union (EBU) and National Television System Committee (NTSC) for the blue illuminant, provided that the coordinates for the standard EBU blue illuminant are (0.15, 0.06) and those for the standard NTSC blue illuminant are (0.14, 0.08). Figure 6 depicts the CIE chromatographic diagram, and the corresponding '*x*' and '*y*' coordinates of pristine and blended LC cells, as well as the corresponding color purity, are listed in Table 1, which represents the color changes induced by the stimuli shown in Figure 6. The noteworthy result of these experiments is that the addition of GNSs into the system has increased the color purity significantly from 65.6 to 95.4%. Observations of the host E7 LC's luminescence properties suggest that the intensity and luminescence color remain constant while GNS concentrations are increased in the environment. This implies that the dispersion of GNSs in the E7 LC does not result in any color shifts in the LC cell, despite the fact that the LC cell has higher absorbance as well as better and enhanced emissivity due to the GNS dispersion.

3.2. Electro-Optical Study. In order to evaluate various electro-optical parameters useful for display applications, we intended to study the transmission spectra of pristine E7 and GNS-blended LC cells which are shown in Figure 7a. The transmission spectra of the GNS-blended LC cells are nearly identical to those of the pristine E7 cell at GNS concentrations of less than 5.0×10^{13} GNSs. When the GNS concentration reaches its optimum value; i.e., 5.0×10^{13} GNSs, the transmission spectra of the GNS-blended LC cell reduce by ~6% due to light scattering, because dispersed GNSs disrupt LC alignment near their surface and scatter a significant amount of incident light. The minor reduction in transmission spectra implies that the dispersion generated by the blended

https://doi.org/10.1021/acsomega.2c06718
ACS Omega 2023, 8, 2315−2327

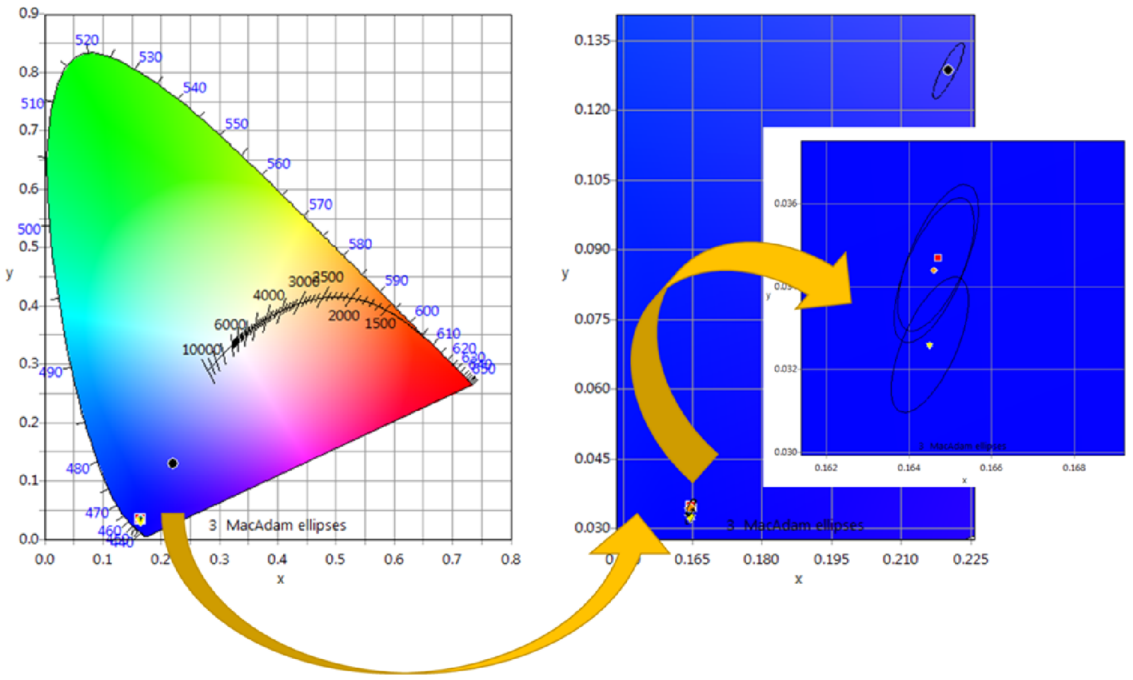

Figure 6. CIE Chromaticity diagram for pure and PEG-capped GNS-dispersed E7 LC cells.

Table 1. CIE Coordinates and Color Purity Datasheet for Pure and Blended E7 LC Cells

LC cell	CIE coordinates		color purity (in %)
	x-coordinate	*y*-coordinate	
pristine E7	0.2202	0.1285	64.6
E7 + 5.0 × 10^{11} GNSs	0.1647	0.0347	94.9
E7 + 5.0 × 10^{12} GNSs	0.1646	0.0344	95.0
E7 + 2.5 × 10^{13} GNSs	0.1645	0.0326	95.4
E7 + 5.0 × 10^{13} GNSs	0.1645	0.0326	95.4

GNSs is insignificant. The GNS solution employed has a crimson red color impression. The low GNS concentration doped in the nematic host is responsible for the missing resonance peak in Figure 7a. As demonstrated in Figure 7b, the transmissions of the 5.0 × 10^{13} GNS-blended cell with incident light at polarization directions of 0° (rubbing direction), 45°, 90°, and 135°, respectively, practically remain constant. As a result of the low GNS dopant, the transmission of the GNS-blended LC cell is polarization independent. The maximum transmission via E7 LC has somewhat decreased for the modest applied field since the addition of GNSs, which could be explained by increased light scattering and/or a change in the refractive index. The threshold voltage (V_{th}) is utilized to calculate the ratio of the electric torque, which connects to dielectric anisotropy and tries to realign the director field, to the restoring elastic torque, which is associated with bulk elasticity. A certain change in V_{th} caused by doping can then be understood as a change in bulk elasticity, dielectric anisotropy, or even both. The transmission versus voltage (T−V) spectra of pristine E7 and GNS-blended LC cells at RT are shown in Figure 7c. The V_{th} and operating voltage (V_{op}) were significantly reduced by the tiny amount of GNS dispersion, as evidenced by a modest shift in the V−T curves observed with increasing GNS concentrations. The measurement of V_{th} has been performed using different methodologies discussed already in our previously published articles,[41,42] and at RT, we found a significant decrease (∼24%) in the value of V_{th} (from about 1.00 to 0.76 Volts) for the pristine E7 LC and LC−GNS composites across all four approaches. Also, ∼12% decrement in the value of V_{op} (from about 2.16 to 1.90 Volts) for pristine E7 and E7/GNS-blended LC cells. This reduction of threshold voltage is probably due to the coupling of electron wave oscillations in GNSs with incident light propagating through the system. Their interaction creates a much higher field inside the sample near the surface of these nanospheres which not only increases the optical tilt of NLC molecules manifold but also lowers V_{th} significantly.[23]

Reduction in threshold voltage is accompanied by lowering of the order parameter of the mesogenic system. For the validation of this fact, we measured the order parameter using two different techniques, one being the macroscopic Haller's extrapolation method and the other being microscopic dichroism method, and their outcomes are discussed below.

3.2.1. Haller's Extrapolation Method. The Haller's approximation expresses the variation of temperature-dependent order parameter by eq 1:[43]

$$S_{\text{Haller's}} = \left(1 - \left(\frac{T}{T_C}\right)\right)^{\beta} \quad (1)$$

where β is the LC material's characteristic constant, and T_C is its clearing temperature. The birefringence is related to the order parameter (S) of LC, and it can be calculated by eq 2:

$$S_{\text{Haller's}} = \frac{\Delta n}{\Delta n_0} \quad (2)$$

Here, Δn is the birefringence at particular temperature and Δn_o is the birefringence at the absolute zero temperature for perfect ordering obtained from Haller's approximation method. The validity of eqs 1 and 2 is that the ambient temperature (T) is sufficiently lesser than that of anisotropic temperature (T_C).[44,45] The linear curve fitting method may be used to calculate the values of Δn_o and β (Table 2). To

https://doi.org/10.1021/acsomega.2c06718
ACS Omega 2023, 8, 2315−2327

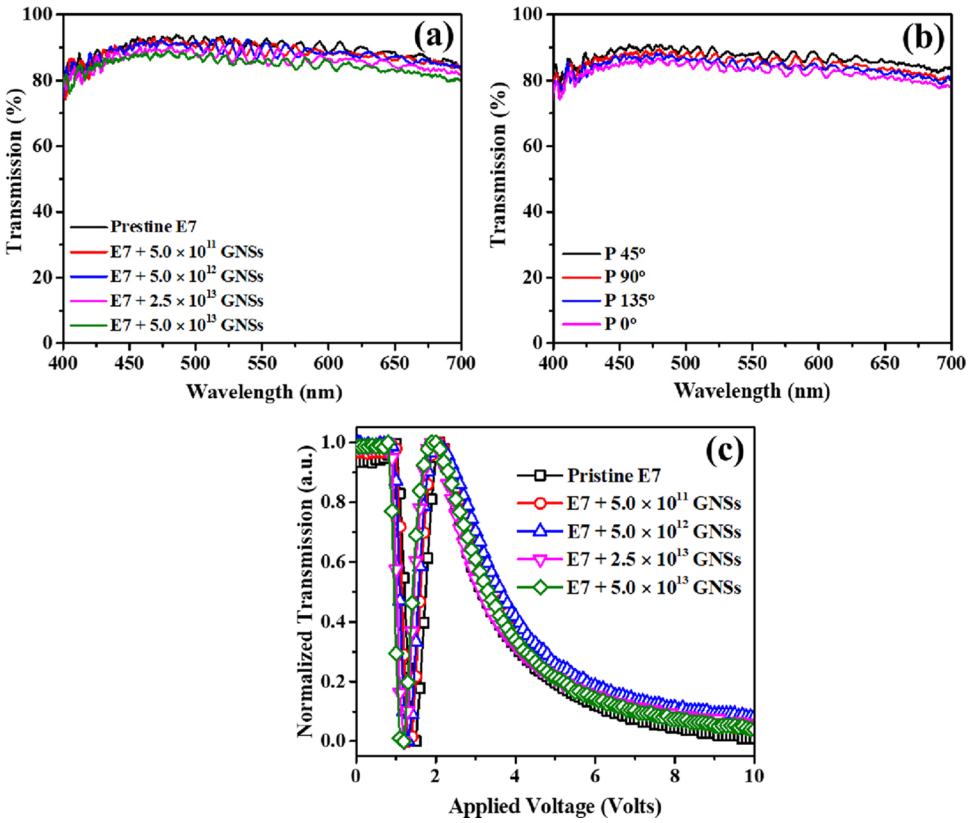

Figure 7. (a) Transmission spectra of the pristine E7 and GNS-blended LC cells, (b) transmission spectra of the 5.0×10^{13} GNS-blended LC cell with incident light at the polarization directions of 0° (rubbing direction), 45°, 90°, and 135°, respectively, and (c) $T-V$ curves for the pristine E7 and GNS-blended LC cells at RT.

Table 2. Fitting Parameters Obtained from Haller's Extrapolation Method for Pristine and GNS-Blended E7 Systems

GNS concentration	Δn_0	T_C (K)	β (degrees)
pristine E7	0.3106 ± 0.24%	334.65 ± 0.028%	0.176 ± 0.593%
E7 + 5.0×10^{11}	0.3086 ± 0.15%	334.15 ± 0.035%	0.189 ± 0.061%
E7 + 5.0×10^{12}	0.2964 ± 0.25%	333.15 ± 0.062%	0.193 ± 0.074%
E7 + 2.5×10^{13}	0.2887 ± 0.50%	331.65 ± 0.047%	0.198 ± 1.124%
E7 + 5.0×10^{13}	0.2793 ± 0.48%	331.15 ± 0.057%	0.169 ± 0.032%

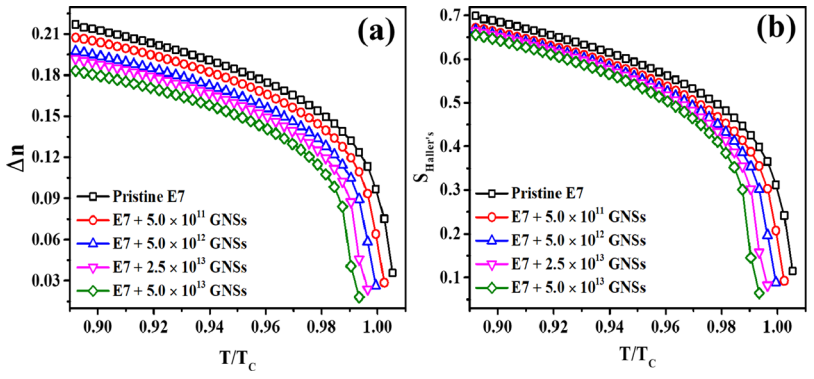

Figure 8. (a) Temperature dependence of birefringence and (b) order parameter of pristine and GNS-blended E7 systems.

determine birefringence using this method, we examined the temperature dependence of birefringence, and Figure 8a depicts this temperature dependence of the birefringence (Δn) for the pristine and GNS-blended E7 systems. With the addition of GNSs to nematic LCs, we observed a significant reduction in birefringence. We observed 4.41, 8.97, 11.62, and 15.62% decrease for E7 blends with 5.0×10^{11}, 5.0×10^{12}, 2.5×10^{13}, and 5.0×10^{13} number of GNSs. This decrease in birefringence of the pristine LC with GNS dispersion can be attributed to a decrease in the value of the orientational order parameter of nematic molecules.

Figure 8b depicts the variation of order parameter with temperature for pristine and GNS-blended E7 systems. The order parameter reduces as the concentration of GNSs

https://doi.org/10.1021/acsomega.2c06718
ACS Omega 2023, 8, 2315−2327

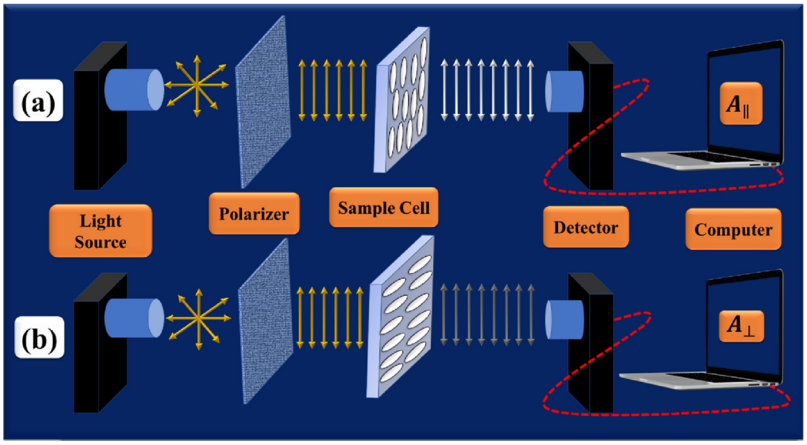

Figure 9. Schematic illustration of the experimental setup used to record polarized absorption spectra of aligned guest−host samples; (a) for measuring absorbance with the LC cell oriented so that the sample is parallel ($A_{\parallel}$) and (b) for measuring absorbance with the LC cell oriented so that the sample is perpendicular ($A_{\perp}$).

increases. Based on this concept and the presumption that there is sufficient connection between the LC molecules and the ligands of the GNSs, the anisometric host will impose a tactoidal deformation of the ligand (according to the suggested model discussed later). It alters the geometry of nanonematic composites in a way that throws off the composite's orientational ordering. As a result, we obtain the decrease in the order parameter due to birefringence. It has an effect on the geometry of nanonematic composites, causing the orientational ordering of the composite to be disrupted. As a consequence, we show that the birefringence, and therefore, the order parameter decrease.

3.2.2. Absorption Band Dichroism Method. The optical band absorption dichroism measurement technique (UV or IR) was used to investigate the order parameter S of a uniaxial LC.[46] The optical technique has proven to be the easiest and most often used method. The order parameter in this approach is defined by three parameters: N, β, and g as:[47]

$$S = \left(\frac{gN - 1}{gN + 2}\right)\left(\frac{1}{1 - \frac{3}{2}\sin^2\beta}\right) \tag{3}$$

where N is the dichroic ratio estimated at a resonant (UV or IR) absorption band, β is the angle subtended between this dipole moment and long molecular axis, and g is a correction factor resulting from the anisotropy of the light wave's local field. The following are the general approaches for assessing S: (1) estimating N of a dipole moment with known β, (2) computing g from molecular geometry, and (3) calculating S from N, β, and g using eq 3. After obtaining S and g, β of each other oscillator in the molecule may be estimated by measuring N at its resonant wavelength. The OD ratio D [$(D = -\log_{10}T$, $T = \exp(\alpha d))$ where T is the transmission of LC layer of thickness d and absorption coefficient α] for light polarized parallel ($\|$) or perpendicular ($\perp$) to the LC direction is known as the dichroic ratio N of an LC layer. The ratio of the absorption coefficient at two orthogonal polarizations is comparable to the following definition (eq 4):

$$N = \left(\frac{D_{\|}}{D_{\perp}}\right) = \left(\frac{\alpha_{\|}}{\alpha_{\perp}}\right) \tag{4}$$

Precise measurements of α are necessary for an accurate estimation of N. In the experiment, the LC layer thickness of 10−15 μm is often employed to estimate the absorption dichroism and found that thicker LC layers are most suitable for this method. In the thin LC layer the transmission is also low; therefore, in a low transmission, any inaccuracy in the experiment or small variation in the substrates can result in substantial error in α, and hence in N and S. Polarization-dependent absorption coefficients were determined in this research. The order parameter of the E7 LC was determined using the absorption dichroism of the C≡N bonds.

The transmittance of an LC cell in the polarizer-LC cell arrangement is expressed as:

$$t = t_p(1 - R)^2\exp(-2\alpha_s L)\exp(-\alpha d) \tag{5}$$

where the transmittance of the polarizer is represented by t_p, R and α_s represent the reflectivity and absorption coefficient of the substrate at wavelength λ_0, L is the thickness of the substrate, d is the thickness of the LC layer, and α is the absorption coefficient of the LC at wavelength λ. The scattering loss due to long-range director variation can be ignored in eq 5, for the aforementioned reasons:

1. The scattering coefficient of the E7 LC mixture (where 5CB is the predominant component) at λ = 632.8 nm with beam diameter ∼2 mm is $\sim 10^{-3}$ μm^{-1}. Thus, at λ = 4450 nm, the scattering loss for a 5 μm-thick (pure) LC layer is approximated to be $\sim 10^{-6}$ of the incident power.[48]
2. We are involved in absorption at the molecular vibrational resonance. Consequently, α is expected to be considerably large, and the scattering loss becomes negligible.

Interfacial reflections inside the LC cell are also ignored in eq 5 because the index mismatch between KCl ($n \sim 1.4856$) and LC ($n \sim 1.5224$) in the visible region is small.[49] Moreover, the absorption loss caused by the KCI substrates is relatively small [$\alpha_s \sim 10^{-3}$ cm^{-1} thus for a 5 μm-thick substrate $\exp(-2\alpha_s L) \sim 0.997$] requiring only the reflection losses caused by the air−substrate interfaces to be addressed.

In general, the alignment of a guest material within a LC host is studied by placing the guest−host mixture in a cell with coated surfaces that cause the bulk sample to align in a defined

https://doi.org/10.1021/acsomega.2c06718
ACS Omega 2023, 8, 2315−2327

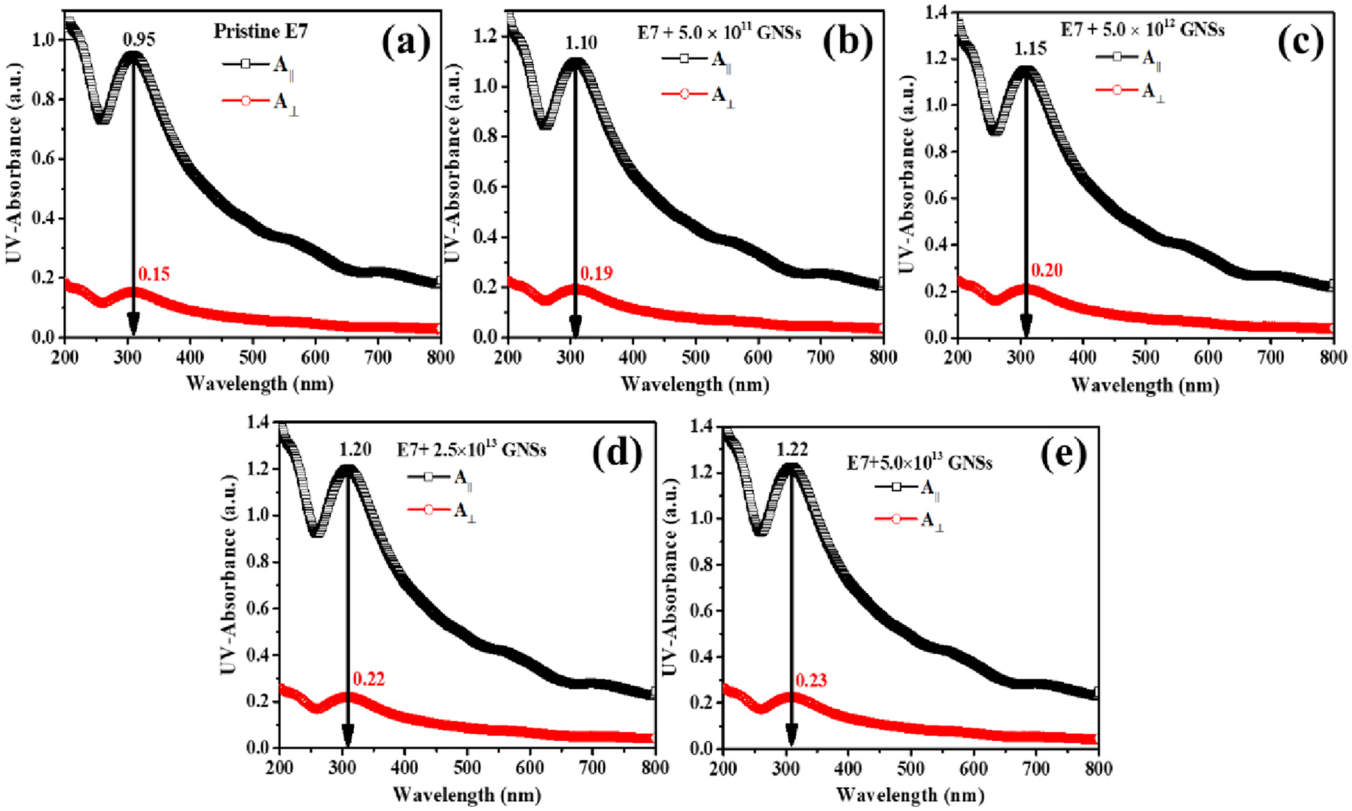

Figure 10. Polarized UV−visible absorption spectra of aligned samples (a) pristine E7 LC and (b) 5.0×10^{11}, (c) 5.0×10^{12}, (d) 2.5×10^{13}, and (e) 5.0×10^{13} number of GNS-blended E7 systems.

Table 3. Parallel and Perpendicular Absorbance, Dichroic Ratio, Dichroic, Haller's Order Parameter, and Percentage Difference

GNS concentration	$A_{\parallel}$	$A_{\perp}$	R	S_{Dichroic}	$S_{\text{Haller's}}$	difference (%)
pristine E7	0.95	0.15	6.33	0.64	0.6988	7.25
E7 + 5.0×10^{11}	1.10	0.19	5.79	0.62	0.6723	7.46
E7 + 5.0×10^{12}	1.15	0.20	5.75	0.61	0.6666	7.57
E7 + 2.5×10^{13}	1.20	0.22	5.45	0.60	0.6645	9.09
E7 + 5.0×10^{13}	1.22	0.23	5.30	0.59	0.6557	9.23

direction, and then measuring the absorbance with the LC cell oriented so that the sample is parallel ($A_{\parallel}$) and then perpendicular ($A_{\perp}$) to the electric vector of incident polarized light. The experimental setup for the measurement using this technique has been demonstrated in Figure 9, and the observed polarized absorption spectra are shown in Figure 10 for the pure E7 LC cell and those blended with different concentrations of GNSs.

The experimental dichroic ratio, $R = \frac{A_{\parallel}}{A_{\perp}}$, is derived from the ratio of these values of absorbance, and it is used to determine the experimental dichroic order parameter of the E7/GNS-blended LC cell by using eqs 6−8

$$S_{\text{Dichroic}} = \frac{R-1}{R+2} = \frac{A_{\parallel} - A_{\perp}}{A_{\parallel} + 2A_{\perp}} \tag{6}$$

$$A_{\parallel} = \varepsilon c l \frac{1}{3}(2S+1) \tag{7}$$

$$A_{\perp} = \varepsilon c l \frac{1}{3}(1-S) \tag{8}$$

where ε is the absorption coefficient of the visible absorption band of the GNS, c is the concentration of the guest material, and l is the path length of the cell. This dichroic order parameter is commonly used to quantify alignment in guest−host systems. $S_{\text{Dichroic}} = 1$ in a perfectly aligned system because the absorbance is zero when the sample is aligned perpendicular to the incident polarized light and $R = \infty$, whereas $S_{\text{Dichroic}} = 0$ in a fully isotropic system because the polarized absorbance does not change when the sample is rotated and $R = 1$. This order parameter should preferably be at least 0.75 for a guest−host system to be suitable for use in a simple display device, though even higher values are preferable because the contrast ratio obtained when switching a device increases with increasing order parameter.[50]

However, it is worth mentioning that the change in values of the order parameter depends on the measurement technique owing to different assumptions about the local field. The dichroic method is used to determine the microscopic order parameter, which is calculated using different quantities than the macroscopic one. Because the effect of the local field differs on different properties, the values calculated for the microscopic and macroscopic order parameters will differ and the

https://doi.org/10.1021/acsomega.2c06718
ACS Omega 2023, 8, 2315−2327

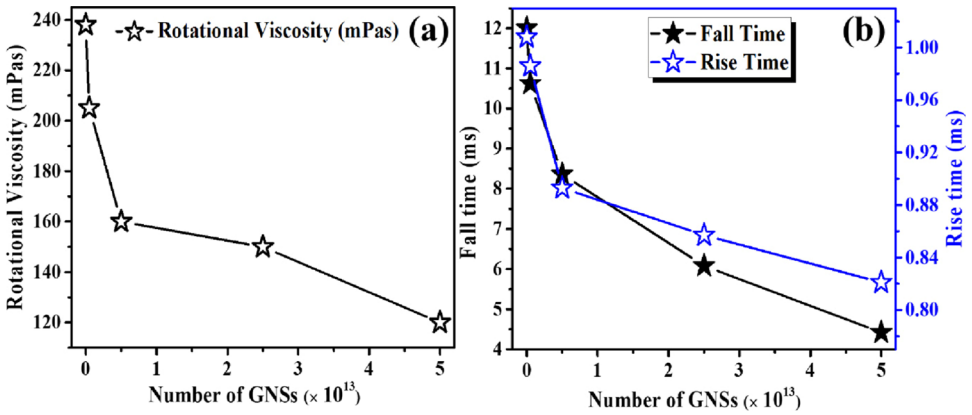

Figure 11. (a) Variation of rotational viscosity and (b) dynamic response of the pristine E7 with different GNS concentrations.

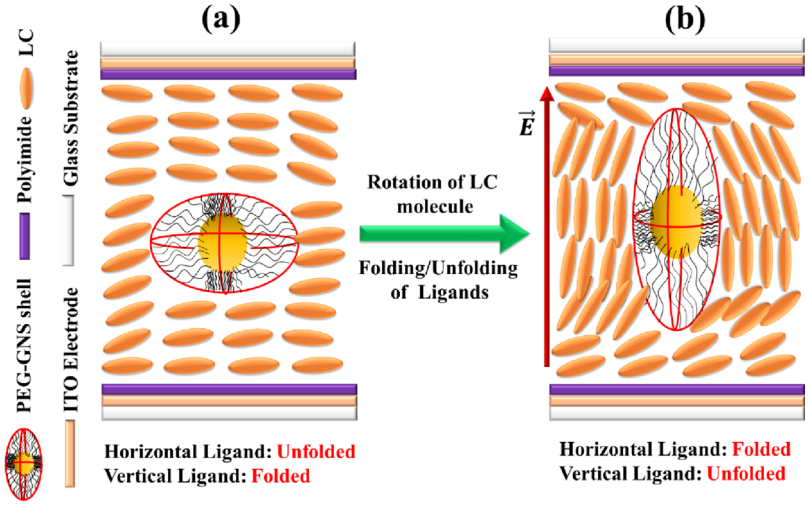

Figure 12. Estimated model of enabled switching due to GNS dispersion is depicted schematically. (a) Anisometric interactions with the LC host deform the ligand shell into a tactoidal shape. (b) When an electric field is applied, the LC molecules rotate, but the nanosphere remains unrotated. Formerly folded ligands unfold, while previously unfolded ligands fold.

comparison of the measured values of the order parameter by these two techniques is tabulated in Table 3. The microscopic dichroic order parameter is derived with refractive indices and molecular polarizability while Haller's approach achieves macroscopic order parameter involving structure parameters of LCs in the calculations. Also, the effective geometry parameter model includes the refractive indices in the relevant equation. All of the above approaches yield an order parameter that is temperature-dependent. As a result, the main difference between the Dichroic and Haller's approaches is indeed the simultaneous temperature dependence of molecular polarizability and refractive index, which results in a small and negligible difference in the values obtained at temperatures far from the T_C when compared to the other two mentioned approaches. The approaches of Dichroic and Haller reveal a slight decrease in the order parameter of the E7/GNS-dispersed system as compared to pristine E7 ($S_{Dichroic}\downarrow$ = ~8 % and $S_{Haller's}\downarrow$ = ~6.17%).

Figure 11 depicts rotational viscosity (γ) (a) and dynamic response (b) of pristine E7 and E7/GNS-blended hybrid cells at RT. The response times of rotational molecular orientation of pristine E7 and LC/GNS composite systems were acquired through the measurement of transient current induced by a direct-current step voltage and from optical transmission data.[51] To understand the effect of PEG-capped GNSs on the dynamic response of LC molecules, study of rotational viscosity in a GNS-blended cell is important, which is closely related to the rotational motion of the LC. The present investigation reveals that the value of γ decreased by 13.86, 32.77, 36.97, and 49.58% for 5.0×10^{11}, 5.0×10^{12}, 2.5×10^{13}, and 5.0×10^{13} number of GNS-blended LC cells respectively.

Figure 11b shows the field-induced switching response for both pure E7 and E7/GNS-blended hybrid cells at various concentrations. The rise time (τ_{on}) and fall time (τ_{off}) of pure and E7/GNS-blended LC cells are found to be decreased in the present investigation. The value of τ_{on} is decreased by 2.18, 11.41, 14.98, and 18.55% for 5.0×10^{11}, 5.0×10^{12}, 2.5×10^{13}, and 5.0×10^{13} number of GNS-blended LC cells, respectively. A significant decrease in τ_{off} is also observed by 11.50, 30.33, 49.33, and 63.17% for 5.0×10^{11}, 5.0×10^{12}, 2.5×10^{13}, and 5.0×10^{13} number of GNSs blended LC cells respectively. The proposed model shown in Figure 12 is used to explain the decrease in τ_{on}, τ_{off}, γ, and k_{11} (see Supporting Information, Table S1).

GNS doping appears to reduce the measured rotational viscosities (γ) (see Figure 11a) and elastic constants (k_{eff}) (see Supporting Information, Table S1). We used a model to explain the decreased viscosity and elastic constant, as well as the decreased threshold voltage. The anisometric host will impose a tactoidal deformation of the ligand based on this

https://doi.org/10.1021/acsomega.2c06718
ACS Omega 2023, 8, 2315−2327

Table 4. Comparative Study of NLC−GNS Composite Systems for Different Capping Agents[a]

nematic LC details	AuNP details		major findings (at RT)	references
	diameter	capping agent		
E7	$d \sim 5$ nm	polyvinyl pyrrolidone (PVP)	$\tau_{on}\downarrow \sim 9\%$; $\tau_{off}\downarrow \sim 24\%$; response time$\downarrow \sim 28\%$; $V_{th}\downarrow \sim 21\%$; $T_{NI}\downarrow$; $S\downarrow$; $\Delta n\downarrow$ slightly; $K\downarrow$; $\Delta\varepsilon\uparrow \sim 5.5\%$; $\eta\downarrow$	Hsu et al.[53]
E7 and 5CB	$d \sim 5$ nm	azo-C11-SH ligands	for E7: $\Delta\varepsilon\downarrow \sim 30\%$; $K_1\downarrow \sim 17\%$; rotational viscosity $\gamma_1\downarrow$; for 5CB: $\Delta\varepsilon\downarrow \sim 40\%$; $K_1\downarrow \sim 32\%$; rotational viscosity γ_1 first ↑, then ↓ with increasing concentration from 1 wt % to 3 wt %	Brouckaert et al.[54]
E7	$d \sim 5$ nm	dodecanethiol ligand shell	relaxation frequency $f_\delta\downarrow$ slightly; $T_{NI}\downarrow$ 1.4 °C.	Bourg et al.[55]
5CB	$d \sim 6$ nm	4-sulfanylphenyl-4-[4-(octyloxy)phenyl]benzoate (SOPB)	8 nm red shift of SPR in absorption edge; $T_{NI}\uparrow \sim 0.4$ °C; $V_{th}\downarrow \sim 25\%$; $S\uparrow$ slightly	Khatua et al.[56]
5CB	NP1: $d \sim 2.4$ nm, NP2: $d \sim 5$ nm	NP1: dodecanethiol ligand shell and NP2: mesogenic ligands	resistivity↓; conductivity↑; $V_{th}\uparrow$; $\varepsilon\uparrow$	Lagerwall and Urbanski[57]
5CB	$d \sim 1.6$−3.1 nm		$T_{NI}\uparrow \sim 3.3$ °C; $\Delta\varepsilon\downarrow$; $V_{th}\downarrow \sim 61\%$; $K_{11}\downarrow$; $\tau_{off}\uparrow$; relaxation frequency $f_\delta\uparrow$; activation energy $E_a\downarrow$	Pandey et al.[58]
5CB	$d \sim 12$ nm	MEO2MA and OEGMA (9:1)	$V_{th}\downarrow \sim 8\%$; light modulatiuon achieved due to light scattering	Hadjichristov et al.[59]
5CB	$d \sim 1.5$−5.2 nm	alkylthiol capping	$T_{NI}\downarrow$; conductivity↑; $\Delta\varepsilon \sim$ unaffected	Krishna Prasad et al.[60]
weakly polar D_5AOB	$d \sim 13$ nm	polyvinyl pyrrolidone (PVP)	$T_{NI}\downarrow \sim 5.5$ °C; $K_{11}\downarrow \sim 23\%$; $\gamma\downarrow \sim 68\%$; response time$\downarrow \sim 57\%$; $V_{th}\downarrow \sim 27\%$; $E_a\downarrow$; $\Delta\varepsilon\uparrow$; $\Delta n\downarrow \sim 23\%$; UV−Vis absorbance$\uparrow \sim 76\%$; OD↑; PL intensity$\uparrow \sim 46\%$	Singh et al.[29,61]
E7	$d \sim 18$ nm	polyethylene glycol (PEG)	$V_{th}\downarrow \sim 24\%$; $\tau_{off}\downarrow \sim 63.17\%$; rotational viscosity$\downarrow \sim 49.58\%$; PL intensity$\uparrow \sim 4$-fold, UV absorbance↑, color purity for display purposes$\uparrow \sim 95.4\%$	current study

[a]Here, ↑ represents an increase in values and ↓ represents a decrease in values.

model and the assumption that there is adequate interaction between the LC molecules and the ligands of the GNSs.[52]

This anisometric shape is believed to be the result of ligand chain folding or coiling in the axial position of the GNS, whereas ligands in the equatorial region fully extend or unfold. When external electric fields are applied, small deformations in the surrounding director field can cause a flip in the equatorial and axial orientation, causing coils to unfold and unfolded ligands to fold up. By means of anisometric interactions between the ligands and the host molecules, the presence of the GNS facilitates the reorientation of the host molecules even in the absence of a rotation of the nanoshell (NS) core. This model would best explain the reduced V_{th} and the rotational viscosity in dispersions with GNS.

As a result, the easier it is to create a distorted ligand shell, the more likely it is that an altered electro-optical (EO) response will be observed. This can be interpreted as a dynamic feedback system in which the effectiveness of an NS to change the EO response is determined by how the LC host can affect it. Thus, the detailed analysis of PEG-functionalized GNSs blended NLC cell has been performed, and a comparative study of nematic LCs dispersed with GNSs of various sizes stabilized with a variety of capping agents has been presented in Table 4.

4. CONCLUSIONS

The optical and EO investigation of PEG-functionalized GNS-blended NLCs was carried out for different concentrations of GNSs in the system. It was observed that the GNS-blended E7 LC material seems to be very beneficial in future photonic and display application as the system possesses various attributes like enhanced luminescence, decreased threshold voltage, fairly good order parameter, decreased rotational viscosity, and stabilized EL. The hyperchromic shift obtained in the UV−visible spectroscopic findings due to the SPR inherent to GNSs makes the system a promising candidate not only for optical devices but also for biomedical applications employing photothermal properties of the system. Apart from that, the system also experiences a great enhancement in the color purity from 64.6 to 95.4% as depicted from CIE results which increases its utility for better display features in the devices. Exclusively superior EO attributes such as lowering of threshold voltage by 24% and reduction in fall time by around 63% make it a favorable option to be employed in the next-generation photonic devices.

■ ASSOCIATED CONTENT

Supporting Information

The Supporting Information is available free of charge at https://pubs.acs.org/doi/10.1021/acsomega.2c06718.

The molecular structure of the E7 LC mixture with its constituents of the different monomers, schematic representation of polyethylene glycol-functionalized GNSs, and polarized optical micrographs of bright and dark state and data on measured values of dielectric parameters (PDF)

■ AUTHOR INFORMATION

Corresponding Authors

Kamal Kumar Pandey − *Department of Physics, Shri Jai Narain Misra Post Graduate College, Lucknow 226001, India;* orcid.org/0000-0002-4171-0784; Email: kamalpande27@gmail.com

Rajiv Manohar − *Liquid Crystal Research Laboratory, Department of Physics, University of Lucknow, Lucknow 226007, India;* orcid.org/0000-0002-7441-8042; Email: rajiv.manohar@gmail.com

Authors

Bhupendra Pratap Singh − *Liquid Crystal Research Laboratory, Department of Physics, University of Lucknow, Lucknow 226007, India;* orcid.org/0000-0002-0383-708X

https://doi.org/10.1021/acsomega.2c06718
ACS Omega 2023, 8, 2315−2327

Samiksha Sikarwar − *Integrated Basic Science, School of Physical and Decision Science, Babasaheb Bhimrao Ambedkar University, Lucknow 226025, India;* orcid.org/0000-0002-7238-0503

Shikha Agarwal − *Liquid Crystal Research Laboratory, Department of Physics, University of Lucknow, Lucknow 226007, India;* orcid.org/0000-0002-7762-3308

Dharmendra Pratap Singh − *Université du Littoral Côte d'Opale, UR 4476, UDSMM, Unité de Dynamique et Structure des Matériaux Moléculaires, Calais 62228, France*

Complete contact information is available at: https://pubs.acs.org/10.1021/acsomega.2c06718

Author Contributions

[⊥]B.P.S. and S.S. contributed equally to this work.

Notes

The authors declare no competing financial interest.

■ ACKNOWLEDGMENTS

The INSPIRE-AORC Program of the Department of Science and Technology (DST), New Delhi [File No. DST/INSPIRE Fellowship/2016/IF160572] is gratefully acknowledged by the author B.P.S. for providing financial assistance in the form of an INSPIRE Fellowship.

■ REFERENCES

(1) Lesiak, P.; Bednarska, K.; Lewandowski, W.; Wojcik, M.; Polakiewicz, S.; Baginski, M.; Osuch, T.; Markowski, K.; Orzechowski, K.; Makowski, M.; Bolek, J.; Wolinski, T. R. Self-Organized, One-Dimensional Periodic Structures in a Gold Nanoparticle-Doped Nematic Liquid Crystal Composite. *ACS Nano* **2019**, *13*, 10154−10160.

(2) Kuang, Z. Y.; Fan, Y. J.; Tao, L.; Li, M. L.; Zhao, N.; Wang, P.; Chen, E. Q.; Fan, F.; Xie, H. L. Alignment Control of Nematic Liquid Crystal using Gold Nanoparticles Grafted by the Liquid Crystalline Polymer with Azobenzene Mesogens as the Side Chains. *ACS Appl. Mater. Interfaces* **2018**, *10*, 27269−27277.

(3) Chang, C.-H.; Lin, R.-J.; Tien, C.-L.; Yeh, S.-M. Enhanced photoluminescence in gold nanoparticles doped homogeneous planar nematic liquid crystals. *Adv. Condens. Matter Phys.* **2018**, *2018*, 1−5.

(4) Bednarska, K.; Lesiak, P.; Orzechowski, K.; Osuch, T.; Markowski, K.; Wojcik, M.; Lewandowski, W.; Wolinski, T.Self-organizing, one-dimensional periodic structures in 5CB doped with gold nanoparticles. In *13th Conference INTEGRATED OPTICS-Sensors, Sensing Structures and Methods IOS*; 2018; p 20.

(5) Asiya, S.; Pal, K.; Kralj, S.; Thomas, S.Nanomaterials dispersed liquid crystalline self-assembly of hybrid matrix application towards thermal sensor. In *Nanofabrication for Smart Nanosensor Applications*; Elsevier, 2020; pp 295−321.

(6) Pal, K.; Sajjadifar, S.; Abd Elkodous, M.; Alli, Y. A.; Gomes, F.; Jeevanandam, J.; Thomas, S.; Sigov, A. Soft, self-assembly liquid crystalline nanocomposite for superior switching. *Electron. Mater. Lett.* **2019**, *15*, 84−101.

(7) Liu, B.; Yang, T.; Mu, X.; Mai, Z.; Li, H.; Wang, Y.; Zhou, G. Smart Supramolecular Self-Assembled Nanosystem: Stimulus-Responsive Hydrogen-Bonded Liquid Crystals. *Nanomaterials* **2021**, *11*, 448.

(8) Vimal, T.; Pujar, G.; Agrahari, K.; Inamdar, S. R.; Manohar, R. Nanoparticle surface energy transfer (NSET) in ferroelectric liquid crystal−metallic-silver nanoparticle composites: Effect of dopant concentration on NSET parameters. *Phys. Rev. E* **2021**, *103*, No. 022708.

(9) Tripathi, S.; Ganguly, P.; Haranath, D.; Haase, W.; Biradar, A. Optical response of ferroelectric liquid crystals doped with metal nanoparticles. *Appl. Phys. Lett.* **2013**, *102*, No. 063115.

(10) Bitar, R.; Agez, G.; Mitov, M. Cholesteric liquid crystal self-organization of gold nanoparticles. *Soft Matter* **2011**, *7*, 8198−8206.

(11) Tong, X.; Xiang, J.; Lu, X.; Karsenti, P.-L.; Zhao, Y. Electrically enhancing and modulating the photoluminescence of upconversion nanoparticles using liquid crystals. *J. Mater. Chem. C* **2018**, *6*, 7683−7688.

(12) Shen, Y.; Dierking, I. Perspectives in liquid-crystal-aided nanotechnology and nanoscience. *Appl. Sci.* **2019**, *9*, 2512.

(13) Jin, S.; Harris, R. D.; Lau, B.; Aruda, K. O.; Amin, V. A.; Weiss, E. A. Enhanced rate of radiative decay in CdSe quantum dots upon adsorption of an exciton-delocalizing ligand. *Nano Lett.* **2014**, *14*, 5323−5328.

(14) Barbosa, J. A.; Abreu, V. L.; Rodrigues, S. S. M.; Frigerio, C.; Santos, J. L. A CdTe−MPA quantum dot fluorescence enhancement flow method for chlorhexidine determination. *Anal. Methods* **2014**, *6*, 4240−4246.

(15) Rodrigues, S. S. M.; Ribeiro, D. S.; Molina-Garcia, L.; Medina, A. R.; Prior, J. A.; Santos, J. L. Fluorescence enhancement of CdTe MPA-capped quantum dots by glutathione for hydrogen peroxide determination. *Talanta* **2014**, *122*, 157−165.

(16) Kumar, A.; Prakash, J.; Mehta, D.; Biradar, A.; Haase, W. Enhanced photoluminescence in gold nanoparticles doped ferroelectric liquid crystals. *Appl. Phys. Lett.* **2009**, *95*, No. 023117.

(17) Chaudhry, M.; Ghildyal, D. Characterization of thermal, electro optical and photoluminescent properties of nematic liquid crystal doped with gold nano particles. *Mater. Today: Proc.* **2022**, *57*, 2061−2066.

(18) Mehrzad, H.; Habibimoghadam, F.; Mohajerani, E.; Neyts, K.; Mohammadimasoudi, M. Tunable, polarized and deeply modulated photoluminescence based on gold nano-islands and liquid crystal. *Opt. Commun.* **2019**, *445*, 119−124.

(19) Chen, C.-T.; Liu, C.-C.; Wang, C.-H.; Chen, C.-W.; Chen, Y.-F. Tunable coupling between exciton and surface plasmon in liquid crystal devices consisting of Au nanoparticles and CdSe quantum dots. *Appl. Phys. Lett.* **2011**, *98*, 261918.

(20) Abdullah, L. A.; Rashad, A. A.; Jber, N. R.; Mahmood, A. I.; Ibrahim, R. K. The Influence of Gold Nanoparticles on Linear and Nonlinear Optical Properties of Liquid Crystal. *J. Southwest Jiaotong Univ.* **2019**, *54*, 1−6.

(21) Vardanyan, K. K.; Sita, D. M.; Walton, R. D.; Saidel, W. M.; Jones, K. M. Cyanobiphenyl liquid crystal composites with gold nanoparticles. *RSC Adv.* **2013**, *3*, 259−273.

(22) Choudhary, A.; Singh, G.; Biradar, A. M. Advances in gold nanoparticle−liquid crystal composites. *Nanoscale* **2014**, *6*, 7743−7756.

(23) Kaur, S.; Singh, S. P.; Biradar, A. M.; Choudhary, A.; Sreenivas, K. Enhanced electro-optical properties in gold nanoparticles doped ferroelectric liquid crystals. *Appl. Phys. Lett.* **2007**, *91*, No. 023120.

(24) Wang, L.; Li, Q. Stimuli-Directing Self-Organized 3D Liquid-Crystalline Nanostructures: From Materials Design to Photonic Applications. *Adv. Funct. Mater.* **2016**, *26*, 10−28.

(25) Feng, X.; Sosa-Vargas, L.; Umadevi, S.; Mori, T.; Shimizu, Y.; Hegmann, T. Discotic Liquid Crystal-Functionalized Gold Nanorods: 2- and 3D Self-Assembly and Macroscopic Alignment as well as Increased Charge Carrier Mobility in Hexagonal Columnar Liquid Crystal Hosts Affected by Molecular Packing and $\pi-\pi$ Interactions. *Adv. Funct. Mater.* **2015**, *25*, 1180−1192.

(26) Pezzi, L.; De Sio, L.; Veltri, A.; Placido, T.; Palermo, G.; Comparelli, R.; Curri, M. L.; Agostiano, A.; Tabiryan, N.; Umeton, C. Photo-thermal effects in gold nanoparticles dispersed in thermotropic nematic liquid crystals. *Phys. Chem. Chem. Phys.* **2015**, *17*, 20281−20287.

(27) Roy, A.; Singh, B. P.; Yadav, G.; Khan, H.; Kumar, S.; Srivastava, A.; Manohar, R. Effect of gold nanoparticles on intrinsic material parameters and luminescent characteristics of nematic liquid crystals. *J. Mol. Liq.* **2019**, *295*, No. 111872.

(28) Jayoti, D.; Malik, P. Dielectric study of gold nanoparticle doped polymer dispersed liquid crystal. *AIP Conf. Proc.* **2018**, *1953*, 100085.

(29) Singh, B. P.; Sikarwar, S.; Agrahari, K.; Tripathi, S.; Gangwar, R. K.; Manohar, R.; Pandey, K. K. Electro-optical characterization of a weakly polar liquid crystalline compound influenced polyvinyl pyrrolidone capped gold nanoparticles. *J. Mol. Liq.* **2021**, *325*, No. 115172.
(30) Budaszewski, D.; Chychlowski, M.; Budaszewska, A.; Bartosewicz, B.; Jankiewicz, B.; Wolinski, T. R. Enhanced efficiency of electric field tunability in photonic liquid crystal fibers doped with gold nanoparticles. *Opt. Express* **2019**, *27*, 14260−14269.
(31) Lin, X.; Ye, S.; Kong, C.; Webb, K.; Yi, C.; Zhang, S.; Zhang, Q.; Fourkas, J. T.; Nie, Z. Polymeric Ligand-Mediated Regioselective Bonding of Plasmonic Nanoplates and Nanospheres. *J. Am. Chem. Soc.* **2020**, *142*, 17282−17286.
(32) Dumur, F.; Dumas, E.; Mayer, C. R. Functionalization of gold nanoparticles by inorganic entities. *Nanomaterials* **2020**, *10*, 548.
(33) Roca, M.; Pandya, N. H.; Nath, S.; Haes, A. J. Linear Assembly of Gold Nanoparticle Clusters via Centrifugation. *Langmuir* **2010**, *26*, 2035−2041.
(34) Kim, D.; Park, S.; Lee, J. H.; Jeong, Y. Y.; Jon, S. Antibiofouling Polymer-Coated Gold Nanoparticles as a Contrast Agent for in Vivo X-ray Computed Tomography Imaging. *J. Am. Chem. Soc.* **2007**, *129*, 7661−7665.
(35) Singh, B. P.; Huang, C.-Y.; Singh, D. P.; Palani, P.; Duponchel, B.; Sah, M.; Manohar, R.; Pandey, K. K. The scientific duo of TiO2 nanoparticles and nematic liquid crystal E204: Increased absorbance, photoluminescence quenching and improving response time for electro-optical devices. *J. Mol. Liq.* **2021**, *325*, No. 115130.
(36) Singh, B. P.; Pathak, G.; Roy, A.; Hegde, G.; Tripathi, P. K.; Srivastava, A.; Manohar, R. Investigation of dielectric and electro-optical properties of nematic liquid crystal with the suspension of biowaste-based porous carbon nanoparticles. *Liq. Cryst.* **2019**, *46*, 1808−1820.
(37) Baur, G.; Wittwer, V.; Berreman, D. Determination of the tilt angles at surfaces of substrates in liquid crystal cells. *Phys. Lett. A* **1976**, *56*, 142−144.
(38) Mie, G. A contribution to the optics of turbid media, especially colloidal metallic suspensions. *Ann. Phys.* **1908**, *25*, 377−445.
(39) Ross, B.; Tasoglu, S.; Lee, L. Plasmon resonance differences between the near- and far-field and implications for molecular detection. *Proc. SPIE* **2009**, *7394*, 739422.
(40) Guo, Y.; Shi, D.; Luo, Z.-W.; Xu, J.-R.; Li, M.-L.; Yang, L.-H.; Yu, Z.-Q.; Chen, E.-Q.; Xie, H.-L. High Efficiency Luminescent Liquid Crystalline Polymers Based on Aggregation-Induced Emission and "Jacketing" Effect: Design, Synthesis, Photophysical Property, and Phase Structure. *Macromolecules* **2017**, *50*, 9607−9616.
(41) Singh, B. P.; Sikarwar, S.; Pandey, K. K.; Duraisamy, S.; Gupta, S. K.; Manohar, R. Nematic Liquid Crystals Dispersed with Thermoelectric Gallium Oxide (Ga2O3) Microrods: A Perspective for Improving the Response Time of Electro-Optical Devices. *J. Phys. Chem. C* **2022**, *126*, 15924−15935.
(42) Singh, B. P.; Sikarwar, S.; Manohar, R.; Shah, A.; Singh, D. P.; Herman, J.; Pandey, K. K. Nematic liquid crystals blended ferroelectric nanoparticles (BaTiO3): A perspective way for improving the response time and photoluminescence for electro-optical devices. *J. Appl. Phys.* **2022**, *131*, 174102.
(43) Balasubramanian, V.; Ramya, A.; Radjarejesri, S.; Vijayakumar, V. Optical and thermal characterization of thermotropic hydrogen bonded liquid crystal mixture. *Mater. Today: Proc.* **2021**, *47*, 1731−1735.
(44) Tough, R. J. A.; Bradshaw, M. J. The determination of the order parameters of nematic liquid crystals by mean field extrapolation. *J. Phys.* **1983**, *44*, 447−454.
(45) Scharf, T.*Polarized light in liquid crystals and polymers*; John Wiley & Sons, 2007.
(46) Saupe, A. Ultraviolet, infrared and magnetic resonance spectroscopy on liquid crystals. *Mol. Cryst. Liq. Cryst.* **1972**, *16*, 87−104.
(47) Saupe, A.; Maier, W. Methods for determining the degree of ordering of nematic crystalline liquid layers. *J. Nat. Res. A* **1961**, *16*, 816−824.
(48) Wu, S.-T.; Lim, K.-C. Absorption and scattering measurements of nematic liquid crystals. *Appl. Opt.* **1987**, *26*, 1722−1727.
(49) Li, J.; Wen, C.-H.; Gauza, S.; Lu, R.; Wu, S.-T. Refractive indices of liquid crystals for display applications. *J. Displ. Technol.* **2005**, *1*, 51.
(50) Bahadur, B.*Liquid crystals: applications and uses*; World Scientific; 1990; vol. *1*.
(51) Chen, H.-Y.; Lee, W.; Clark, N. A. Faster electro-optical response characteristics of a carbon-nanotube-nematic suspension. *Appl. Phys. Lett.* **2007**, *90*, No. 033510.
(52) Draper, M.; Saez, I. M.; Cowling, S. J.; Gai, P.; Heinrich, B.; Donnio, B.; Guillon, D.; Goodby, J. W. Self-Assembly and Shape Morphology of Liquid Crystalline Gold Metamaterials. *Adv. Funct. Mater.* **2011**, *21*, 1260−1278.
(53) Hsu, C.-J.; Lin, L.-J.; Huang, M.-K.; Huang, C.-Y. Electro-optical Effect of Gold Nanoparticle Dispersed in Nematic Liquid Crystals. *Crystals* **2017**, *7*, 287.
(54) Brouckaert, N.; Podoliak, N.; Orlova, T.; Bankova, D.; De Fazio, A. F.; Kanaras, A. G.; Hovorka, O.; D'Alessandro, G.; Kaczmarek, M. Nanoparticle-Induced Property Changes in Nematic Liquid Crystals. *Nanomaterials* **2022**, *12*, 341.
(55) Bourg, M.; Urbanski, M. Spectroscopic insight into molecular fluctuations and phase stability of nematic composites containing gold nanoparticles or carbon nanotubes. *Phys. Chem. Chem. Phys.* **2017**, *19*, 23302−23308.
(56) Khatua, S.; Manna, P.; Chang, W.-S.; Tcherniak, A.; Friedlander, E.; Zubarev, E. R.; Link, S. Plasmonic Nanoparticles−Liquid Crystal Composites. *J. Phys. Chem. C* **2010**, *114*, 7251−7257.
(57) Urbanski, M.; Lagerwall, J. P. F. Nanoparticles dispersed in liquid crystals: impact on conductivity, low-frequency relaxation and electro-optical performance. *J. Mater. Chem. C* **2016**, *4*, 3485−3491.
(58) Pandey, A. S.; Dhar, R.; Kumar, S.; Dabrowski, R. Enhancement of the display parameters of 4′-pentyl-4-cyanobiphenyl due to the dispersion of functionalised gold nano particles. *Liq. Cryst.* **2011**, *38*, 115−120.
(59) Hadjichristov, G. B.; Marinov, Y. G.; Petrov, A. G.; Bruno, E.; Marino, L.; Scaramuzza, N. Electro-optically responsive composites of gold nanospheres in 5CB liquid crystal under direct current and alternating current joint action. *J. Appl. Phys.* **2014**, *115*, No. 083107.
(60) Krishna Prasad, S.; Sandhya, K. L.; Nair, G. G.; Hiremath, U. S.; Yelamaggad, C. V.; Sampath, S. Electrical conductivity and dielectric constant measurements of liquid crystal−gold nanoparticle composites. *Liq. Cryst.* **2006**, *33*, 1121−1125.
(61) Singh, B. P.; Sikarwar, S.; Tripathi, S.; Agarwal, S.; Sah, M.; Manohar, R.; Pandey, K. K. Thermodynamic and spectroscopic characterization of a weakly polar liquid crystalline compound dispersed with polyvinyl pyrrolidone capped gold nanoparticles. *J. Mol. Liq.* **2022**, *354*, No. 118889.

https://doi.org/10.1021/acsomega.2c06718
ACS Omega 2023, 8, 2315−2327